STRESS AND DEFORMATION OF A CELL BY OPTICAL STRETCH

Chuan Li*, Y. P. Liu, A. C. K. Lai

School of Mechanical and Aerospace Engineering, Nanyang Technological University 50 Nanyang Ave. Singapore 639798

*mcli@ntu.edu.sg

Abstract

The mechanical behavior of erythrocytes is studied both experimentally and numerically. In the experimental part, prepared silica microbeads are attached to the surface of spherically swollen erythrocytes (red blood cells, RBCs) in a suspension. The cells are then stretched by single laser beam via the microbeads. A relation between the stretching force and cell deformation is quantitatively assessed. Meanwhile, a physical model for an axisymmetric cell is introduced to study its deformation by different level of stretching force. By comparing the experimental and numerical data, stiffness of the cell membrane can be determined and the optimal values are found to agree with other studies by different techniques such as micropipette aspiration or high frequency electric field.

Introduction

Laser trapping has been widely used to manipulate small objects ranging from atoms to living cells in many research areas such as biology, medicine, physics and engineering. The trapping force is due to the radiation pressure in electromagnetic field, generated by photons' momentum [1-3]. The magnitude of such force is on the order of one to hundreds piconewtons (pN) from most commercially available systems.

The simplest instrument among all is the single beam laser trap, called optical tweezers, which is a very useful tool in the study of cell biology. One example is the study of mechanical behavior of erythrocytes suspended in buffer solution [4]. In this study, a single laser trapped erythrocyte will rotate and re-orientate until it reaches an equilibrium position. A relationship between the torque and angle of orientation can be established from the experimental data. Dharmadhikari [5] also reported the re-orientation of malaria-infected RBCs by laser trapping in the buffer solution. They found the original biconcave disk shape of erythrocyte was folded into a rod-like shape after deformation.

One advantage of laser trapping is that it is a non-destructive method of measuring overall material response to the external loadings because the force field can be directly applied on the cell without destroying it. In order to pin point down the force location, a highly focused laser beam is preferred. However, the smallest focus can be made is dictated by the wavelength of laser. Typical wavelengths for trapping purpose are 1064, 980 and 830 nm. Shorter wavelength could penetrate the membranes of cell and nucleus to damage the DNA and kill the cell.

For a selected wavelength, the cell can be targeted more easily and accurately by the laser beam if a small microbead attached to its surface as the marker [6-8]. This approach reduces the directly shining of laser beam on the cell and thus avoid cell being deformed by the radiation pressure. Moreover, the microbeads can be used as handles since they are smaller and much stiffer than cells.

In this paper, an experiment study on the deformation of erythrocytes by single laser beam stretch is carried out. The erythrocytes, specially processed to become spherical shape in a suspension, are mixed up with microbeads for spontaneous adhesion. The deformation of erythrocytes is measured at different level of force. A mechanical model is also introduced to simulate the deformation of erythrocytes. By comparing the experimental and numerical results, the stiffness modulus of cell membrane is predicted quantitatively.

Experiment

Cell and Microbead Preparation

Fresh blood was drawn from white rats and stored in acid citrate dextrose (Sigma C3821) at 4℃ in refrigerator. An aliquot of blood sample was first diluted in phosphate-buffered saline (PBS, Sigma P4417) then rinsed and fractionated by centrifugation three times. Similarly, silica microbeads purchased from Bangs Laboratories (Fishers, IN, US) were rinsed in deionized water and centrifugated for several times. The repetitive wash for RBCs and microbeads is to ensure the spontaneous adhesion between RBCs and microbeads in later processes.

The washed RBCs and microbeads were diluted again by PBS to the concentration of $\sim 1\times10^5/\mu l$ and $\sim 2\times10^5/\mu l$ respectively. After diluting, $20\mu l$ of each suspension was mixed together in a little vial. The equal amount is intended to make every two beads adhered to one erythrocyte. The mixed suspension was incubated at 4°C for 1 hour to allow spontaneous and nonspecific adhesion between the microbeads and RBCs [3, 6-8]. After the adhesion between RBCs and beads were confirmed under an optical microscope, the suspension of mixture was further diluted to $\sim 1\times10^3$ cells/μl in a hypotonic buffer (10mM potassium phosphate, pH7.4, 75mM NaCl, i.e., 155mOsm/kg), with a small amount (~1mg/ml) of Bovine serum albumin (BSA, Sigma

ISSN: 1727-1983

A4503) added to prevent RBCs from sticking to the glass plate [6]. This suspension should be kept for about 10~20 minutes before the experiment of laser trapping can be started, for allowing RBCs to swell into spherical or nearly spherical shape.

Optical tweezers

A schematic drawing of the optical tweezers is shown in Fig.1. The whole system was purchased from Cell Robotics Inc., NM, US. Source of laser is Nd:YAG and pumped by a 1.5W diode. Laser is then reflected through dichroic mirrors and focused by an inverted microscope (Nikon optical microsystem) before it reaches the objects. The wavelength of 1064nm is chosen to minimize the absorption by water and hemoglobin. This is to avoid the possible damage due to the heating by laser on trapped RBCs [9].

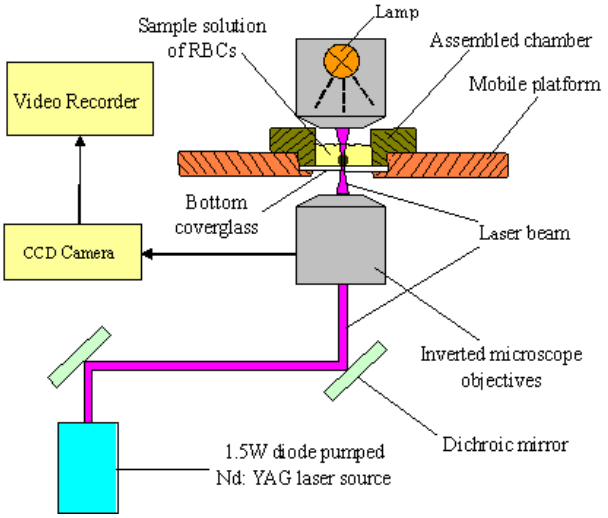

Fig.1 Schematic drawing of the optical tweezers (Module 1064/1500 from Cell Robotics Inc.).

The chamber for observation is assembled of glass slides and coverslips. Prior to the experiment, all slides and coverslips were treated with BSA (100mg/ml). In addition, the bottom glass slides were silanized with Dichlorodimethylsilane solution ($C_2H_6C_{l2}Si$, Sigma 85126) [10]. Dichlorodimethylsilane solution is commonly used in protein analysis for silanizing the glass to prevent sticking of proteins [10].

Force Calibrations

Our main purpose of this experimental study is to find the relation between external loading and cell deformation. Though the force cannot be measured directly, it can be calibrated with the input power of laser. Using silica beads only, we can trap the beads by laser and let the fluid flow over it. At a certain power level, there is a maximum fluid velocity beyond that the trapping force can no longer hold the beads. This is an equilibrium state where the trapping force is balanced by the viscous drag force [11]. Therefore, following the Stokes' flow, the trapping force is

$$F = 6\pi R\eta V \qquad (1)$$

where R is the radius of microbeads, η the liquid viscosity (1.01×10^{-3} Pa·sec at 25℃ for water) and V the maximum velocity directly measured by the system from its motor speed.

Fig.2 shows the calibration of trapping force vs. input power of laser with a linear curve fitting. This linear relation was explained earlier by Lenormand et al [11]. The relative accuracy in the calibration is estimated to be ~10% mainly due to the uncertainty in microbeads' size. Note that all observations and measurements were made at room temperature in the laboratory (~25℃).

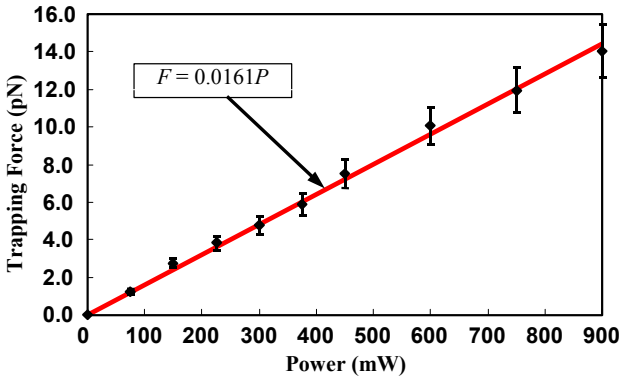

Fig.2 Force calibration by dragging a silica bead (2.34mm in dia.) in Stoke's flow at the maximum escape velocity.

Image Processing

In order to measure the deformation of erythrocytes, each photo taken by CCD camera is digitally processed by the MATLAB. Since the average size of microbeads is known (2.34μm in dia.), our main task is to find the edges of erythrocytes and microbeads in each photo and measured their distance in pixels. Based upon the known size of microbeads, a conversion between the pixels and the real physical length can be established in a statistical way by randomly measuring any two opposite points on the perimeter of a bead. This mapping is fairly accurate as long as the measures are made at many different locations. For example, the conversion is found to be 0.023237 μm/pixel for the cell no.1 in Table 1.

Experimental Results

Experimental results of five example cells are shown in Fig. 3 along with selected images. Corresponding values of all measurements are listed in Table 1. The geometry of cells is measured by image processing as mentioned previously. The stretching force is calculated by the correlation of the trapping force and input power from Fig. 2. For accuracy, we specifically carried out experiments each time at different force level for each cell instead of running through the whole range from 2 to 15 pN. Note that the radius of attachment δ by beads is also measured and tabulated. This small dimension has to be included later in the mechanical modeling. To further quantify the experimental results, a transverse (ε_t) and longitudinal strain (ε_l) are introduced as following

$$\varepsilon_t = \frac{\Delta D}{D_0} = \frac{D_0 - D}{D_0} \qquad (2)$$

ISSN: 1727-1983

$$\varepsilon_l = \frac{\Delta L}{D_0} = \frac{L - D_0}{D_0} \qquad (3)$$

where D_0 is the original diameter ($=2R$) of RBCs before deformation; D is the maximum length perpendicular to the stretching direction and L the maximum length parallel to the stretching. To avoid confusion, Eq. (2) and (3) are specifically defined to make both strains positive. It is found that the transverse strain in this study is easier to identify and measured than the longitudinal one due to the attachment by beads. Fig. 3 demonstrates a positive correlation between the stretching force and transverse strain for five selected cells. In other words, the more stretching, the more elliptic cell could become.

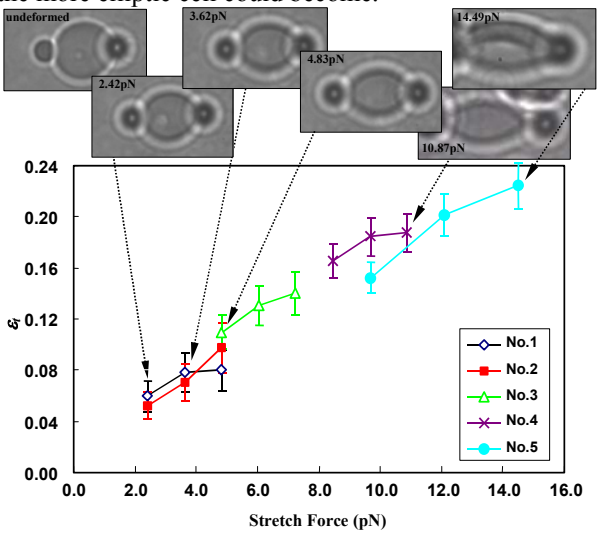

Fig.3 Experimental data and images of deformed RBCs with attached silca microbeads (3.204mm in dia.) at different stretching forces.

Mechanical Modeling

Erythrocytes are known to have a simpler structure than other mammal cells for that they consists of membrane (phospholipid bi-layer) and cytoplasm (mainly hemoglobin with iron particles) without nucleus or mitochondria. The plasma membrane is stiffer than the cytoplasm and thus maintains the structure integrity. For this reason, RBCs are conventionally represented by their membranes in many mechanical models.

Geometry and Kinematic Relation

Considering a spherical cell membrane with radius a is axisymmetrically deformed along the stretching direction (z*-direction, cf. Fig. 4). Introducing two non-dimensional coordinates: $r^* = r/a$, $z^* = z/a$, $s^* = s/a$ and $R^* = R/a$, $Z^* = Z/a$ $S^* = S/a$ for the membrane before and after deformation respectively, then the followings have to be valid [15].

$$r^* = \sin s^* \qquad (4)$$

$$z^* = 1 - \cos s^* \qquad (5)$$

$$\frac{dR^*}{dS^*} = \cos\varphi \qquad (6)$$

$$\frac{dZ^*}{dS^*} = \sin\varphi \qquad (7)$$

where φ is the meridional angle, s and S are arc lengths before and after deformation. Note that s^* is exactly the meridional angle φ because $s = a\varphi$.

Also, we can have two dimensionless, principal curvatures of membrane in the meridional (s or φ) and circumferential (θ) as [15]

$$\kappa_s^* = a\kappa_s = \frac{d\varphi}{dS^*} \qquad (8)$$

$$\kappa_\theta^* = a\kappa_\theta = \frac{\sin\varphi}{R^*} \qquad (9)$$

Note that $\kappa_s = \kappa_\theta = \frac{1}{a}$ in the undeformed cell. κ_θ^* can be directly calculated once R^* and φ are determined.

Correspondingly, two principal stretches (strains) along the circumferential (θ) and meridional (s or φ) directions are introduced as [15]

$$\lambda_s = \frac{dS^*}{ds^*} \qquad (10)$$

$$\lambda_\theta = \frac{R^*}{r^*} = \frac{R^*}{\sin s^*} \qquad (11)$$

Physically, the first term represents the change of arc length along the meridional direction and the second term the radius change along the circumferential one.

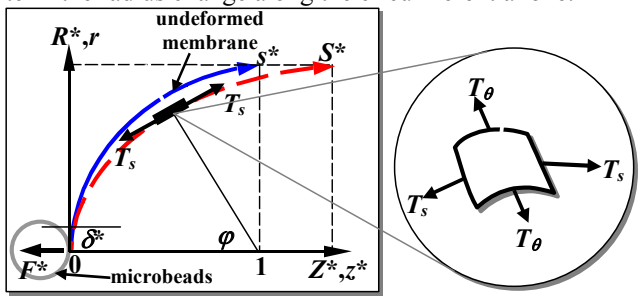

Fig.4 Geometry of the RBC membrane before and after deformation

Constitutive Law

Here we adopted the earlier studies by Pamplona and Calladine [15] on bi-lipid layer to assume there exist resultant tensile forces (N·m^{-1}, T_s and T_θ in Fig. 4) across the membrane thickness in any infinitesimal element. Note that the principal direction is coincident with the circumferential and meridian directions for axisymmetric cases. We can further represent the tensile stresses in terms of the average (T) and deviatoric part as [15]

$$T_s = T + H\frac{1}{\lambda} \qquad (12)$$

$$T_\theta = T + H\lambda \qquad (13)$$

where H is the modulus of stiffness (N·m^{-1}) and

$$\lambda = \lambda_\theta = \lambda_s^{-1} = R^*/\sin s^* = ds^*/dS^* \qquad (14)$$

Note that this relation is valid provided that membrane is incompressible (constant area), i.e. $\lambda_\theta\lambda_s = 1$.

ISSN: 1727-1983

Equilibrium and Governing Equations

Equilibrium equations for the cell membrane can be found from the classical theory for shells [16-17]. For axisymmetry, those equations reduce to two for the tension T^* and curvature κ_s^* along the arc length s^*. Combining the geometric requirements Eq. (6) – (8), we can have the whole set of governing equations in a dimensionless form as

$$\frac{dR^*}{ds^*} = \frac{\cos\varphi \sin s^*}{R^*} \quad (15)$$

$$\frac{dZ^*}{ds^*} = \frac{\sin\varphi \sin s^*}{R^*} \quad (16)$$

$$\frac{d\varphi}{ds^*} = \frac{\kappa_s^* \sin s^*}{R^*} \quad (17)$$

$$\frac{dT^*}{ds^*} = \frac{\cos\varphi - \cos s^*}{R^*} \quad (18)$$

with

$$\kappa_s^* = \frac{-(T^* + \lambda)\cdot \sin\varphi / R^*}{T^* + 1/\lambda} \quad (19)$$

The last two, (18) and (19), are equilibrium equations for tension and curvature with replacements of κ_θ^*, λ_s and λ_θ from (8) – (11). Note that for computational purposes the derivative is changed from the current configuration ($\frac{d}{dS^*}$) back to the original one ($\frac{d}{ds^*}$) by the chain rule in (14). The dimensionless stresses are defined as $T_s^* = T_s / H$, $T_\theta^* = T_\theta / H$ and $T^* = T / H$.

3.4 Boundary Conditions and Numerical Calculations

The boundary conditions were imposed by considering the beads attachment at $s^* = s_0^* = \sin^{-1}\delta^*$,

$$R^*(s_0^*) = \delta^* \quad (20)$$

$$Z^*(s_0^*) = 0 \quad (21)$$

$$\varphi(s_0^*) = \varphi_0 \quad (22)$$

$$T^*(s_0^*) = \frac{F^*}{2\pi\delta^* \sin\varphi_0} - \frac{\sin(s_0^*)}{R^*(s_0^*)} \quad (23)$$

and two-fold symmetry at $s^* = \frac{\pi}{2}$,

$$\varphi(\pi/2) = \pi/2 \quad (24)$$

$$T^*(\frac{\pi}{2}) = \frac{F^*}{2\pi R^*(\pi/2)} - \frac{1}{R^*(\pi/2)} \quad (25)$$

where $F^* = F/aH$ is the dimensionless stretching force and $\delta^* = \delta/a$. Eq. (23) and (25) were obtained by the overall force balance between F and T_s^* around the cell assuming that F are highly concentrated in the adhesion area.

Eq. (15) – (18) together with conditions (20) – (25) form a non-linear, boundary value problem which can be solved by Runge-Kutta method. But to start the procedure, the initial values of φ and κ_s^* at s_0^* have to be guessed. With successive adjustment of both initial values by simplex method to meet the conditions (24) – (25) at $\frac{\pi}{2}$, accurate solutions can be obtained. To facilitate the whole simulations, following starting conditions at s_0^* are recommended also.

$$\frac{dR^*}{ds^*} = \cos\varphi_0 \quad (26)$$

$$\frac{dZ^*}{ds^*} = \sin\varphi_0 \quad (27)$$

$$\frac{d\varphi}{ds^*} = \kappa_s^*(s_0^*) \quad (28)$$

$$\frac{dT^*}{ds^*} = \frac{\cos\varphi_0}{\delta^*} - \frac{\sqrt{1-\delta^{*2}}}{\delta^*} \quad (29)$$

Numerical Solutions

Since δ^* is much smaller than the cell, its variation on the cell deformation is very minor. Using the average value $\delta^* = 0.185$ from Table 1 and the previously proposed numerical scheme, the profile of deformed cell by different stretching force can be obtained as shown in Fig. 5. The higher stretching force, the more elongation of cell in the Z^* direction as expected. The membrane could become concave locally near the adhesion area if stretching is high enough.

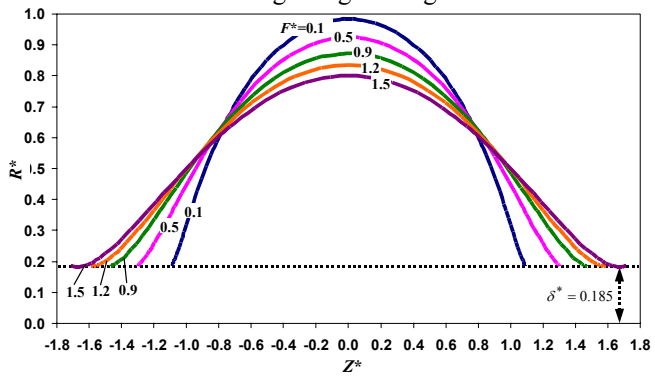

Fig.5 Numerical results for the deformed RBC with microbeads attached ($\delta^* = 0.185$).

Numerical and Experimental Results Comparison

Comparisons of the experimental and numerical results are made based upon the transverse strain ε_t defined earlier in Eq. (2) to find the stiffness H of membrane. It is first noticed that H is a scale to non-dimensionalize the stretching force ($F^* = F/aH$).

ISSN: 1727-1983

Cell No.	Diameters (pixels)	Original radius a (μm)	Trapping force F (pN)	Length of L (pixels)	Length of D (pixels)	average 2δ (pixels)	$\delta^* = \delta/a$	ε_t	ε_l	$H\times10^{-6}$ (N·m^{-1})	Optimal $H\times10^{-6}$ (N·m^{-1})
1	127.606	1.482	2.415	148.082	120.003	25.26	0.198	0.0596	0.1605	**4.1721**	**5.1821**
			3.623	157.295	117.641			0.0786	0.2327	**4.6817**	
			4.830	169.896	117.380			0.0801	0.3314	**6.0700**	
2	138.007	1.602	2.415	156.944	130.750	24.07	0.174	0.0526	0.1372	**4.4048**	**4.5648**
			3.623	173.534	128.250			0.0707	0.2574	**4.8195**	
			4.830	188.858	124.500			0.0979	0.3685	**4.5115**	
3	123.548	1.435	4.830	178.594	110.013	23.71	0.194	0.1096	0.4456	**4.4484**	**4.7484**
			6.038	183.249	107.380			0.1309	0.4832	**4.5559**	
			7.245	188.286	106.250			0.1400	0.5240	**5.0637**	
4	125.841	1.465	8.453	207.580	105.001	23.03	0.184	0.1656	0.6495	**4.7821**	**5.0021**
			9.660	225.143	102.626			0.1845	0.7891	**4.8183**	
			10.868	240.670	102.251			0.1875	0.9125	**5.3194**	
5	142.743	1.657	9.660	181.598	121.000	24.81	0.174	0.1523	0.2722	**5.3063**	**5.0008**
			12.075	197.298	114.000			0.2014	0.3822	**4.7878**	
			14.490	218.007	110.750			0.2241	0.5273	**5.0543**	

Table 1: Experimental measurement of five RBCs

Therefore for each ε_t measured in the experiment, we can determine F^* correspondingly from the numerical solutions in Fig. 5. Then using the measured data of a and F from the 3rd and 4th column in Table 1, the stiffness H can be calculated. Results are shown in the second to last column in Table 1 for every measurement. Conversely, we can find a single value of H for each cell. But this single value cannot completely match all numerical ε_ts from the experiment. Thus, an optimization of

$$\text{Error} = \min\left(\sqrt{\sum_{i=1}^{3}(\varepsilon_{t,\text{exp}}^{i} - \varepsilon_{t,\text{num}}^{i})^2}\right) \qquad (30)$$

has to be solved for every cell to determine an optimal H. The constraint of H is restricted to the maximum and minimum of three Hs for each cell in Table 1. The optimal values of H, listed in the last column of Table 1, results a good correlation between the experiments and computations as shown in Fig. 6. Its range, 4.56~5.18 μN·m^{-1}, is close to the studies in [6] (2.5±0.5 μN·m^{-1}), and [14, 18-20] (4.0~10.0 μN·m^{-1}) for human RBCs measured by other techniques such as micropipette aspiration or high frequency electric field.

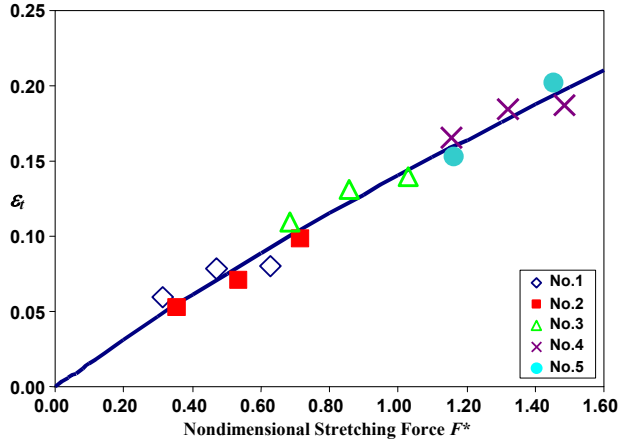

Fig.6 Comparison of numerical and experimental results for deformed RBCs with the optimal tensile stiffness.

Conclusions

In this study, an experimental work of single beam laser stretched erythrocytes was conducted. The erythrocytes were specially treated by buffer solutions to become spherical shape and attached by prepared silica microbeads. The relation of stretching force and cell deformation was quantitatively assessed by the digital image processing. In addition, a mechanical model was introduced to simulate the deformation of cell membrane by stretching. Comparisons of the experimental and numerical data were made by matching a defined transverse strain to determine the stiffness of membrane. An optimal stiffness of each example cell in the experiment was also calculated by minimizing the errors between the experimental and numerical data. The optimal stiffness ranging 4.56~5.18 μN·m^{-1} is very close to those from other studies by different experimental techniques such as micropipette aspiration or high frequency electric field.

References

[1] A. Ashkin, (1998): Methods in Cell Biology 55 pp.1.
[2] S. Chu, (1991): Science, 253 pp.861.
[3] J. Guck, R. Ananthakrishnan, H. Mahmood, T. J. Moon, C. C. Cunningham, J. Kas, (2001): Biophys. J. 81 pp.767.
[4] S. C. Grover, R. C. Gauthier, A. G. Skirtach, (2000): Optics Express 7 pp.533.
[5] J. A. Dharmadhikari, S. Roy, A. K. Dharmadhikari, S. Sharma, D. Mathur, (2004): Optics Express 12 pp.1179.
[6] S. Hénon, G. Lenormand, A. Richert, F. Gallet, (1999): Biophys. J. 76 pp.1145.
[7] J. Sleep, D. Wilson, R. Simmons, W. Gratzer, (1999): Biophys. J. 77 pp.3085.
[8] K. Svoboda, S. M. Block, (1994):Ann. Rev. Biophys. Biomol. Struct. 23, pp.247.

ISSN: 1727-1983

[9] Y. Liu, D. K. Cheng, G. J. Sonek, M. W. Berns, C. F. Chapman, B. J. Tromberg, (1995): Biophys. J. 68 pp.2137.
[10]K. Svoboda, C. F. Schmidt, D. Branton, S. M. Block, (1992): Biophys. J. 63 pp.784.
[11]G. Lenormand, S. Hénon, A. Richert, J. Siméon, F. Gallet, (2001): Biophys. J. 81 pp.43.
[12]E. A. Evans, R. Waugh, L. Melnik, (1976): Biophys. J. 16 pp.585.
[13]R. E. Waugh, E. A. Evans, (1979): Biophys. J. 26 pp.115.
[14]R. M. Hochmuth, R. E. Waugh, (1987): Ann. Rev. Physiol. 49 pp.209.
[15]D. C. Pamplona, C. R. Calladine, (1993): J. Biomech. Eng. 115 pp.149.
[16]W. Flugge, Stresses in Shells, 2nd ed., Springer, New York, 1973.
[17]A. C. Ugural, Stresses in Plates and Shells, 2nd ed., McGraw-Hill, New York, 1999.
[18]E. A. Evans, (1973): Biophys. J. 13 pp.941.
[19]J. C. Lelievre, C. Bucherer, S. Geiger, C. Lacombe, V. Vereycken, (1995): J. de Phsique. III 5 (10) pp. 1689.
[20]H. Engelhardt, E. Sackmann, (1988): Biophys. J. 54 pp.495.

ISSN: 1727-1983